Commun. Comput. Phys.
doi: 10.4208/cicp.210513.091013a

Vol. **15**, No. 5, pp. 1320-1342
May 2014

# A Stability Analysis of Hybrid Schemes to Cure Shock Instability

Zhijun Shen[1,2,*], Wei Yan[1] and Guangwei Yuan[1]

[1] *National Key Laboratory of Science and Technology on Computational Physics, Institute of Applied Physics and Computational Mathematics, P.O. Box 8009-26, Beijing 100088, China.*
[2] *Center for Applied Physics and Technology, HEDPS, Peking University, Beijing 100871, China.*

Received 21 May 2013; Accepted (in revised version) 9 October 2013

Communicated by Kun Xu

Available online 14 February 2014

**Abstract.** The carbuncle phenomenon has been regarded as a spurious solution produced by most of contact-preserving methods. The hybrid method of combining high resolution flux with more dissipative solver is an attractive attempt to cure this kind of non-physical phenomenon. In this paper, a matrix-based stability analysis for 2-D Euler equations is performed to explore the cause of instability of numerical schemes. By combining the *Roe* with *HLL* flux in different directions and different flux components, we give an interesting explanation to the linear numerical instability. Based on such analysis, some hybrid schemes are compared to illustrate different mechanisms in controlling shock instability. Numerical experiments are presented to verify our analysis results. The conclusion is that the scheme of restricting directly instability source is more stable than other hybrid schemes.

**AMS subject classifications**: 35L65, 65M08, 76M12, 76L05

**Key words**: Godunov methods, numerical shock instability, hybrid scheme.

## 1 Introduction

In the last several decades, Godunov-type [6] schemes based on Riemann solvers are among of the most successful methods in computational fluid dynamics (CFD), which exhibit strong robustness in most situations. However, there are some problems in extending Godunov methods to two-dimensional case, for example, the Roe solver [28]

*Corresponding author. *Email addresses:* shen_zhijun@iapcm.ac.cn (Z. Shen), wyanmath01@sina.com (W. Yan), yuan_guangwei@iapcm.ac.cn (G. Yuan)

 

and HLLC solver [31] for the Euler equations may suffer from carbuncle and odd-even decoupling phenomena that are called numerical shock instability [25]. Recently, similar phenomena have been found in shallow water simulations [11].

Several attempts have been made to understand and cure the phenomenon [4, 12, 18, 22, 25, 29, 35]. Quirk [25] gives a one-dimensional analysis and points out the relation between pressure and density perturbations, that is, a scheme will be afflicted by the odd-even decoupling if the perturbation to the pressure field affects the density field. He uses a pressure gradient to detect a shock, and constructs a hybrid method by combining the HLL [9] and Roe [28] schemes to cure shock instability. Pandolfi and D'Ambrosio [22] extend the analysis of the linearized algorithms to several upwind schemes, and then use the information obtained to design remedies to shock instability by slight and local modification to the original schemes (i.e., by imposing an additional linear wave). Gressier and Moschetta adopt similar analysis method [7] to derive a criteria which predicts the odd-even decoupling, and show that the strict stability on Quirk's test is incompatible with the exact resolution of steady contact waves. Sanders et al. [29] notice that the dimension by dimension extension of one-dimensional upwind schemes to the multidimensional equations of gas dynamics often leads to poor results when computing stationary shocks. Through a different linear analysis from Quirk's, they show that this failure is an instability which is the result of inadequate crossflow dissipation implied by strictly upwind schemes. A multidimensional dissipation based on one-dimensional entropy correction is provided to eliminate the instability. Other multidimensional effect is considered in rotational Riemann solver [3, 15, 20, 26]. Ren [26] analyzes dissipative term of linear shear wave, and shows that compared with the grid-aligned flux function, the rotated flux function has more dissipation, and thus it has better stable performance. Liou [18] identifies that the multidimensional shock instability comes from a pressure term in the mass flux. Thus the AUSM schemes whose mass fluxes do not depend on the pressure term are free from carbuncle phenomenon [18, 30]. Furthermore, Park and Kwon [23] point out that the existence of the pressure term in mass fluxes is only a sufficient condition for the scheme being shock-stable. Xu and Li discuss the dissipative mechanism in the Godunov method in [35]. They give an explanation of numerical shock instability by using a formula for quasi-one-dimensional nozzle fluid. Due to the numerical dissipation diminishing in transverse direction of shock wave, the numerical shock instability will appear. Especially in the subsonic region, once there is perturbation inside the numerical shock layer, the instability will happen. In the supersonic region the flow structure is essentially stable with respect to any small perturbation. Recently Jiequan Li et al. [16] compare difference of the generalized Riemann solver and the gas-kinetic scheme for inviscid compressible flow simulations, they regard when the non-equilibrium physical reality in shock layer is replaced by an equilibrium one, the shock instability will be triggered since the equilibrium state used inside a shock layer cannot provide enough numerical dissipation. Dumbser et al. develop a stability analysis for two-dimensional steady shocks based on the matrix method [4]. The background fluid is a steady shock wave instead of a uniform constant state as that in Quirk's analysis. The perturbation is

two dimensional, so the linear analysis has genuinely two dimensional mechanism. With this approach, they indicate that the instability of steady shocks is governed not only by the upstream Mach number but also by the numerical shock structure. The source of the instability is localized in the supersonic region and not in subsonic domain as opposed to Xu's conclusion. Not only such, they find some interesting phenomena such as the Osher method with natural ordering version becomes stable for Mach numbers larger than 5.5. Recently, Dumbser and Toro propose a new version of the Osher-Solomon Riemann solver, which is simpler than the original Osher method and is applicable to general hyperbolic conservation laws [5].

Of all modification methods, the hybrid ones of combining high resolution flux with more dissipative solvers are attractive because it can control certain instabilities by changing the flavor of the dissipation mechanism rather than increasing the absolute level of dissipation. One of the earliest works to combine the HLL and Roe schemes to cure shock instability pertains to Quirk [25]. Even if some schemes with kinetic energy preserving and entropy stable property have to resort to hybrid methods to modify such flaws [1]. To alleviate dissipation, the detection for grid faces deemed as susceptible to the shock instabilities is adopted. Nishikawa and Kitamura use the idea about rotated Riemann solver, and combine two different Riemann solvers to construct a very robust numerical scheme [20]. The rotation of coordinate system is dictated by physical flow features. Wu et al. [34] use a classical and simple hybrid method like Quirk's, but the weight function of hybrid flux scheme is determined by velocity difference across cell edge rather than other criterion such as pressure difference. One new feature is that the effects of flux components are taken into consideration when blending different flux functions. More works are presented in [10, 12, 13, 33].

These works provide some useful explanations and guidelines to prevent shock instability, but some difficult problems are still left unsolved. One example is that there is still no definite clue to show which term or flux is responsible for the anomalies. Liou regards the pressure term in the mass flux is the root of instability [18], however, such viewpoint does not always hold in general. In fact, some AUSM methods without pressure term in mass fluxes suffer shock instabilities [7, 22]. Another example is referred to linear stability analysis conclusions. Carbuncle phenomenon is sometimes described as a transverse numerical instability associated with the shock wave [7, 22, 23, 32]. The conclusion usually comes from linear stability analysis based on uniform constant fluids with even-odd perturbations. But according to the observation and analysis by Dumbser et al. [4], the Roe scheme is unstable only when shock Mach number is over a threshold, therefore, the analysis based on uniform flow is not sufficient and not persuasive. In addition, we are puzzled by the behaviors of some hybrid schemes. For instance, both of the two schemes in [20] and [34] deliver good robustness and high accuracy for many stringent test problems, but the approaches of choosing Riemann solvers in the vicinity of shock (see Fig. 2) are different. The question is which one is more reasonable.

In this paper we attempt to reply to the above questions. We adopt matrix stability analysis method proposed by Dumbser et al. [4], but the emphasis is on the linear stabil-

ities of some hybrid schemes. These schemes use different fluxes or flux components on the different cell edges. By using the combination of different fluxes, we hope to find out which factor influences the behavior of numerical results mostly, such as which terms or components in the numerical fluxes that are responsible for shock instability. Based on the analysis, the causes and consequences of the instability will be investigated. With the instability mechanism understood, the advantage and disadvantage of some hybrid schemes are discussed. Numerical experiments are performed to verify our analysis results, and show that the instability appears for some existing schemes that are claimed as carbuncle-free. Such analysis is helpful for devising better hybrid schemes which can remove some instability and keep accuracy as well.

The paper is organized as follows. Section 2 introduces the fluid equations and some related background about the grid-aligned finite volume method. Two hybrid methods from [20] and [34] are represented in Section 3. The stability analysis with a matrix-based method is described in Section 4, and the analysis results for a series of hybrid schemes are given in Section 5. The stability mechanisms and numerical experiments are presented in Section 6, and finally summary is in Section 7.

## 2 Governing equations and discretization in space

The governing equations of inviscid flow in two-dimension are as follows:

$$\frac{\partial \mathbf{U}}{\partial t}+\frac{\partial F(\mathbf{U})}{\partial x}+\frac{\partial G(\mathbf{U})}{\partial y}=0, \tag{2.1}$$

where the state vector and flux vectors are

$$\mathbf{U}=\begin{bmatrix}\rho\\ \rho u\\ \rho v\\ E\end{bmatrix},\qquad F(\mathbf{U})=\begin{bmatrix}\rho u\\ \rho u^2+p\\ \rho uv\\ u(E+p)\end{bmatrix},\qquad G(\mathbf{U})=\begin{bmatrix}\rho v\\ \rho uv\\ \rho v^2+p\\ v(E+p)\end{bmatrix}.$$

The equation of state is in the form of

$$p=(\gamma-1)\rho e=(\gamma-1)\Big(E-\frac{1}{2}\rho(u^2+v^2)\Big),$$

where $\gamma$ is the specific heat ratio.

We consider some two-dimensional domains in $x$-$y$ space and assume it is discretized into structured quadrilateral control volumes. Examples of typical control cell is shown in Fig. 1. Finite-volume schemes for Eq. (2.1) are obtained by considering the control volume balance equation

$$\frac{d\mathbf{U}_m}{dt}=-\frac{1}{|V_m|}\sum_{k=1}^{4}\int_{A_k}^{A_{k+1}}(T_k^n)^{-1}F(T_k^n\mathbf{U})dA, \tag{2.2}$$

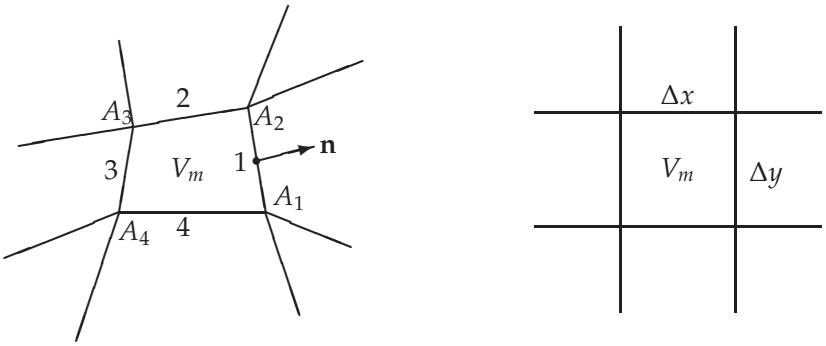


Figure 1: Notations on a quadrilateral grid and a rectangular grid.

where $\mathbf{U}_m$ is the cell average of $\mathbf{U}$ on $V_m$, and $|V_m|$ denotes the volume of $V_m$, and $A_kA_{k+1}(k=1,2,3,4)$ are cell edges. $T_k^n$ is the rotation matrix and $(T_k^n)^{-1}$ is its inverse, namely

$$T_k^n=\begin{pmatrix}1&0&0&0\\0&n_x&n_y&0\\0&-n_y&n_x&0\\0&0&0&1\end{pmatrix},\quad (T_k^n)^{-1}=\begin{pmatrix}1&0&0&0\\0&n_x&-n_y&0\\0&n_y&n_x&0\\0&0&0&1\end{pmatrix}, \tag{2.3}$$

where $\mathbf{n}=(n_x,n_y)$ is the unit outward norm vector of cell $V_m$ on edge $A_kA_{k+1}$.

Assume numerical fluxes $H_{mk}$ between cell $V_m$ and $V_k$ have been constructed, and then we have the semi-discrete conservative scheme as

$$\frac{d\mathbf{U}_m}{dt}=-\frac{1}{|V_m|}\sum_{k=1}^{4}\mathcal{L}_k(T_k^n)^{-1}H_{mk}(T_k^n\mathbf{U}_m,T_k^n\mathbf{U}_k), \tag{2.4}$$

where $\mathcal{L}_k$ is the length of segment $A_kA_{k+1}$.

Denote $\mathbf{Z_m}=T_k^n\mathbf{U}_m$, $\mathbf{Z_k}=T_k^n\mathbf{U}_k$. The numerical flux $H_{mk}(\mathbf{Z_m},\mathbf{Z_k})$ is determined by solving a Riemann problem of one dimensional Euler equations:

$$\frac{\partial\mathbf{U}}{\partial t}+\frac{\partial F(\mathbf{U})}{\partial x}=0.$$

The *Roe* numerical flux is given by

$$H_{mk}^{Roe}(\mathbf{Z_m},\mathbf{Z_k})=\frac{1}{2}\big(F(\mathbf{Z_m})+F(\mathbf{Z_k})-|F'(\hat{Z}_{mk})|(\mathbf{Z_k}-\mathbf{Z_m})\big), \tag{2.5}$$

where $\hat{Z}_{mk}$ denotes the *Roe* average middle state.

The $HLL$ numerical flux is given by

$$H_{mk}^{HLL}(\mathbf{Z_m},\mathbf{Z_k})=\frac{1}{2}\big(F(\mathbf{Z_m})+F(\mathbf{Z_k})-|S_L|(\mathbf{Z}_*-\mathbf{Z_m})-|S_R|(\mathbf{Z_k}-\mathbf{Z}_*)\big), \tag{2.6}$$

where $Z_*$ denotes the middle state of the $HLL$ approximate solution, and $S_L$,$S_R$ are left and right wave velocities, respectively. Due to the existence of absolute value of wave velocities, neither of the two flux solvers is differentiable to $\mathbf{Z_m}$ and $\mathbf{Z_k}$.

## 3 Two hybrid methods

General rotated Riemann solvers are based on the decomposition of the unit normal vector $\mathbf{n}$ at cell edge into two orthogonal directions,

$$\mathbf{n}=\alpha_1\mathbf{n}_1+\alpha_2\mathbf{n}_2,\quad \mathbf{n}_1\cdot\mathbf{n}_2=0, \tag{3.1}$$

where $|\mathbf{n}_1|=|\mathbf{n}_2|=1$, and

$$\alpha_1=\mathbf{n}_1\cdot\mathbf{n},\quad \alpha_2=\mathbf{n}_2\cdot\mathbf{n}. \tag{3.2}$$

If we denote numerical flux $\Phi_{mk}(\mathbf{n})=(T_k^n)^{-1}H_{mk}(T_k^n\mathbf{U}_m,T_k^n\mathbf{U}_k)$, then the cell edge flux is decomposed into the following form:

$$\Phi_{mk}(\mathbf{n})=\alpha_1\Phi_{mk}^{Low}(\mathbf{n}_1)+\alpha_2\Phi_{mk}^{High}(\mathbf{n}_2), \tag{3.3}$$

where $\Phi_{mk}^{Low}$ and $\Phi_{mk}^{High}$ correspond to one dimensional fluxes $H_{Low}$ and $H_{High}$, which can be low and high resolution Riemann solvers or the same approximate solver.

Ren [26] uses the same *Roe* solver, while Nishikawa and Kitamura [20] employ the *Roe* flux function in $\mathbf{n}_2$ and the $HLL$ flux in $\mathbf{n}_1$, that is

$$\Phi_{mk}^{N}=\alpha_1\Phi_{mk}^{HLL}(\mathbf{n}_1)+\alpha_2\Phi_{mk}^{Roe}(\mathbf{n}_2). \tag{3.4}$$

The direction $\mathbf{n}_1$ on edge can be determined by many methods. Ren [26] shows that it is a good choice by taking $\mathbf{n}_1$ as a velocity difference vector between two adjacent cells. Paper [20] makes a slight modification and uses the following form of $\mathbf{n}_1$,

$$\mathbf{n}_1=\begin{cases}\frac{\Delta u\mathbf{i}+\Delta v\mathbf{j}}{\sqrt{\Delta u^2+\Delta v^2}}, & \text{if } \sqrt{\Delta u^2+\Delta v^2}>\varepsilon,\\ \mathbf{n}_\perp, & \text{otherwise,}\end{cases} \tag{3.5}$$

where $\mathbf{i}$ and $\mathbf{j}$ are unit vectors along $x$ and $y$ directions respectively, and $(\Delta u,\Delta v)$ is the velocity difference vector taken over two adjacent cells. $\varepsilon$ is a small parameter. $\mathbf{n}_\perp$ denotes the tangential direction to cell edge. In the case of a grid-aligned shock wave, the combined fluxes on different edges are demonstrated in Fig. 2(a).

A simple hybrid method is used in [34]. Wu et al. avoid the rotated procedure of flux function and make direct combination to different fluxes. The numerical flux is

$$\Phi_{mk}(\mathbf{n})=\beta_1\Phi_{mk}^{High}(\mathbf{n})+\beta_2\Phi_{mk}^{Low}(\mathbf{n}), \tag{3.6}$$

where $\Phi_{mk}^{High}$ takes high resolution scheme such as *Roe* or exact Godunov method and $\Phi_{mk}^{Low}$ is dissipative less wave flux as HLL. $\beta_1$ and $\beta_2$ depend on decomposition of $\mathbf{n}$. But now the direction $\mathbf{n}_1$ in [34] is determined by

$$\mathbf{n}_1=\begin{cases}\frac{\Delta u\mathbf{i}+\Delta v\mathbf{j}}{\sqrt{\Delta u^2+\Delta v^2}}, & \text{if } \sqrt{\Delta u^2+\Delta v^2}>\varepsilon,\\ \mathbf{n}, & \text{otherwise.}\end{cases} \tag{3.7}$$

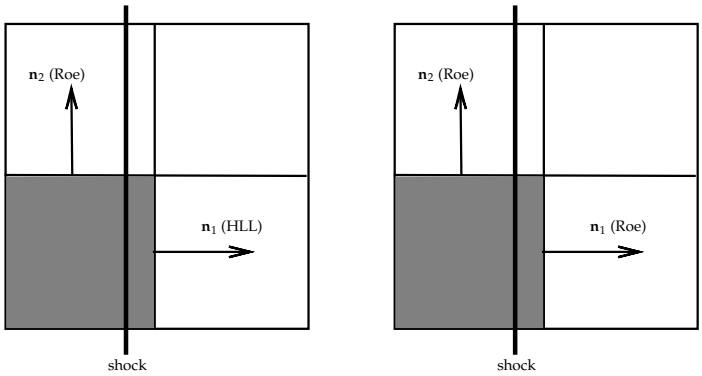


Figure 2: Selected normals for a grid-aligned shock wave: (a) Nishikawa-Kitamura, (b) Wu-Shen-Shen.

This choice is known to select the direction normal to a shock front if shock exists [15]. $\beta_1$ and $\beta_2$ are

$$\beta_1=\alpha_1/(\alpha_1+\alpha_2),\quad \beta_2=1-\beta_1. \tag{3.8}$$

In the case of a grid-aligned shock wave, the combined fluxes on different cell edges are depicted in Fig. 2(b).

In order to reduce dissipation furthermore, Wu-Shen-Shen scheme is proposed in [34], which adopts the following weights and fluxes,

$$\beta_1=\frac{1}{2}+\frac{1}{2}\frac{\alpha_1}{\alpha_1+\alpha_2},\quad \beta_2=1-\beta_1, \tag{3.9}$$

and

$$\begin{cases} H^W_{mk}(1)=\beta_1 H^{Roe}_{mk}(1)+\beta_2 H^{HLL}_{mk}(1),\\ H^W_{mk}(2)=H^{Roe}_{mk}(2),\\ H^W_{mk}(3)=\beta_1 H^{Roe}_{mk}(3)+\beta_2 H^{HLL}_{mk}(3),\\ H^W_{mk}(4)=H^{Roe}_{mk}(4), \end{cases} \tag{3.10}$$

where the index $(i)\,(i=1,2,3,4)$ represents the $i$th component of the flux function $H_{mk}$.

# 4 Linear stability analysis

## 4.1 Matrix stability analysis

A matrix-based stability analysis [4] has been used to study the occurrence of unstable modes during the shock wave computation. For the convenience of further discussion, we describe the approach in [4] once more and add some comments.

For the stability analysis of a steady field, we assume that

$$\mathbf{U}_m = \mathbf{U}_m^0 + \delta\mathbf{U}_m, \tag{4.1}$$

where $\mathbf{U}_m^0$ is the steady mean value and $\delta\mathbf{U}_m$ is small numerical random perturbation.

The flux function can be linearized around the steady mean value as follows

$$H_{mk}(T_k^n\mathbf{U}_m, T_k^n\mathbf{U}_k) = H_{mk}(T_k^n\mathbf{U}_m^0, T_k^n\mathbf{U}_k^0) + \frac{\partial H_{mk}}{\partial \mathbf{Z_m}} T_k^n \delta\mathbf{U}_m + \frac{\partial H_{mk}}{\partial \mathbf{Z_k}} T_k^n \delta\mathbf{U}_k. \tag{4.2}$$

Substituting (4.2) into (2.4) gives

$$\frac{d(\delta\mathbf{U}_m)}{dt} = -\frac{1}{|V_m|}\sum_{k=1}^{4}\mathcal{L}_k(T_k^n)^{-1}\Big(\frac{\partial H_{mk}}{\partial \mathbf{Z_m}} T_k^n \delta\mathbf{U}_m + \frac{\partial H_{mk}}{\partial \mathbf{Z_k}} T_k^n \delta\mathbf{U}_k\Big). \tag{4.3}$$

The first term on the right hand side of (4.3) contains the influence of the error in the cell $m$ itself, and the second term contains the influence of the errors of the four neighbors $k(=1,2,3,4)$ of cell $m$. Equation (4.3) holds for all cells in the computational domain and so we finally get the error evolution of all $M$ cells in the domain.

$$\frac{d}{dt}\begin{pmatrix} \delta\mathbf{U}_1 \\ \vdots \\ \delta\mathbf{U}_M \end{pmatrix} = S\begin{pmatrix} \delta\mathbf{U}_1 \\ \vdots \\ \delta\mathbf{U}_M \end{pmatrix}, \tag{4.4}$$

where $S$ is the stability matrix. When considering only the evolution of initial errors, the solution of the linear time invariant system (4.4) is

$$\begin{pmatrix} \delta\mathbf{U}_1 \\ \vdots \\ \delta\mathbf{U}_M \end{pmatrix} = \exp^{St}\begin{pmatrix} \delta\mathbf{U}_1 \\ \vdots \\ \delta\mathbf{U}_M \end{pmatrix}_0, \tag{4.5}$$

and remains bounded if the maximum of the real part of the eigenvalues of $S$ is negative.

Usually it is not easy to obtain analytically the gradients of the numerical flux functions $\frac{\partial H_{mk}}{\partial \mathbf{Z_m}}$ and $\frac{\partial H_{mk}}{\partial \mathbf{Z_k}}$. [4] evaluated the matrix element of $S$ numerically by a centered difference approximation

$$\frac{\partial H_{mk}}{\partial Z_{mj}} = \frac{H_{mk}(\mathbf{Z}_m + \delta\mathbf{I}_j, \mathbf{Z}_k) - H_{mk}(\mathbf{Z}_m - \delta\mathbf{I}_j, \mathbf{Z}_k)}{2\delta}, \tag{4.6}$$

where $\mathbf{I}_j$ denotes unit vector of which the $jth$ component is 1. Small parameter $\delta = 10^{-7}$. The effect of this variation is not sensitive when $\delta$ is sufficiently small ($< 10^{-6}$), see [4].

In order to modify non-differentiable characteristic of absolute value in (2.5)-(2.6), we replace $|\lambda|$ by a smoothed version of the absolute-value function

$$\phi_{\delta_0}(\lambda) = \begin{cases} |\lambda|, & \text{if } |\lambda| \geq \delta_0, \\ (\lambda^2 + \delta_0^2)/(2\delta_0), & \text{if } |\lambda| < \delta_0, \end{cases}$$

where $\delta_0 = 10^{-4}$. Such smoothing procedure can enhance reliability to stability analysis in theory although most numerical calculations show that it is insensitive to eigenvalue evaluation.

About the matrix stability analysis, there are following properties.

**Remark 4.1.** The linear stability analysis describes the evolvement of perturbation quantities for fluid calculation. It could not reflect whole nonlinear computation procedure, for example, it does not calculate $e = E/\rho - 0.5(u^2+v^2)$ and always assumes that the scheme is positive one. Therefore when an analysis result shows that a scheme is stable, it does not mean the numerical scheme is definitely an appropriate one.

Anyway, the matrix stability analysis is a powerful tool, which shows the quantitative validation to the numerical behavior and illustrates stability mechanism of numerical scheme. When a stability analysis asserts a scheme to be unstable, the instability in Euler computations always can be detected although such unstable phenomenon appears only in some specific numerical examples.

## 4.2 Initial values and boundary conditions

Calculations are performed on a 2D domain $[0,1]\times[0,1]$. The grid is composed of regular Cartesian cells without perturbation. The total cell number is $I \times J$. Here $I = 10, J = 10$.

The raw state is a steady normal shock wave, proposed by Sanders et al. [29]. The initial data are given by the exact Rankine-Hugoniot solution in $x$-direction. The upstream and downstream states are

$$\mathbf{W}_0 = (\rho, u, v, p)_0 = \Big(1, 1, 0, \frac{1}{\gamma M_a^2}\Big), \quad x < 0.5, \tag{4.7}$$

and

$$\mathbf{W}_1 = (\rho, u, v, p)_1 = \Big(f(M_a), \frac{1}{f(M_a)}, 0, \frac{g(M_a)}{\gamma M_a^2}\Big), \quad x > 0.5, \tag{4.8}$$

where $M_a$ is the upstream Mach number, and

$$f(M_a) = \Big(\frac{2}{\gamma+1}\frac{1}{M_a^2} + \frac{\gamma-1}{\gamma+1}\Big)^{-1}, \quad g(M_a) = \frac{2\gamma}{\gamma+1}M_a^2 - \frac{\gamma-1}{\gamma+1}.$$

The initial values are given by slightly random perturbations to all conservative quantities in each cell by the relative order $10^{-6}$.

The boundary conditions in all directions are imposed through ghost cells. The top and bottom boundaries are set to be reflection and left is inflow conditions.

In subsonic region the outflow mass flux is required to be fixed to preserve the initial shock position. That means $(\rho * u)_{R,j} = (\rho * u)_1 = constant$ for $j = 1,2,\cdots,J$, where quantities

$\rho_1$,$u_1$ are known density and velocity without perturbation in subsonic domain. Using characteristic relation for simple wave, the states in ghost cells are

$$\rho_{R,j}=\rho_{I,j},\quad u_{R,j}=\frac{(\rho*u)_1}{\rho_{R,j}},\quad v_{R,j}=v_{I,j}, \tag{4.9a}$$

$$c_{R,j}=\frac{\gamma-1}{2}(u_{I,j}-u_{R,j})+c_{I,j},\quad p_{R,j}=\frac{\rho_{R,j}*c_{R,j}^2}{\gamma}. \tag{4.9b}$$

### 4.3 Notations of hybrid schemes

Numerical fluxes $H_{mk}$ $(k=1,2,3,4)$ on four edges of cell $V_m$ can employ four different schemes (refer to Fig. 1). But here we just use two flux functions: one is in $x$-direction that is normal to shock surface, the other is in $y$-direction that is parallel to shock, which means $H_{m3}$,$H_{m4}$ have same flux formulae as $H_{m1}$ and $H_{m2}$ respectively. For the sake of simplicity, we will refer to this hybrid scheme as $H_{m1}-H_{m2}$.

## 5 Stability of hybrid schemes

### 5.1 Hybridization of the $HLL$ and $Roe$ fluxes

It is well known that the Roe scheme is shock-unstable, while the $HLL$ scheme is stable. To determine which edge flux leads to a shock wave instability for the *Roe* scheme, we consider two hybrid schemes: $Roe-HLLE$ and $HLLE-Roe$. Here the $HLLE$ scheme is a typical example of the $HLL$ solver along with the wave speed estimates proposed by Einfeldt [9]. The eigenvalues of the stability matrix of the steady shock problem at $M_a=7$ are shown in Fig. 3. The $HLL$ and $Roe-HLL$ schemes are carbuncle free but the *Roe* and $HLL-Roe$ are shock-unstable at this shock strength. Through many tests we know that the $Roe-HLL$ and $HLL$ are stable for any Mach number $M_a$. For example, for the $Roe-HLL$, $\max(Re(\lambda))=-0.0789$ at $M_a=200$. The unstable phenomena of the Roe and $HLL-Roe$ appear only for $M_a>2$. This shows that the linear instability is indeed caused by disturbances in the transverse rather than normal direction of shock. To alleviate shock instability a dissipative flux should be added on the cell-edge perpendicular to the shock wave front, but not necessarily on edge parallel to the shock.

Such conclusions have been drawn heuristically in some papers [7, 23, 25, 32] by analyzing one dimensional uniform flow. But from the matrix stability analysis [4] we know the calculation remains stable if upstream Mach number is below a threshold value, therefore the conclusion based on the original analysis for uniform flow is not true unconditionally.

If the $HLL$ and *Roe* fluxes are combined on one edge, the maximum eigenvalue is located between the stable and unstable state. It depends on shock strength and combination coefficients (also called as hybrid parameters). Denote the numerical flux $RoeHLL$ as:

$$H_{mk}^{RoeHLL}=\beta_1 H_{mk}^{Roe}+\beta_2 H_{mk}^{HLL},$$

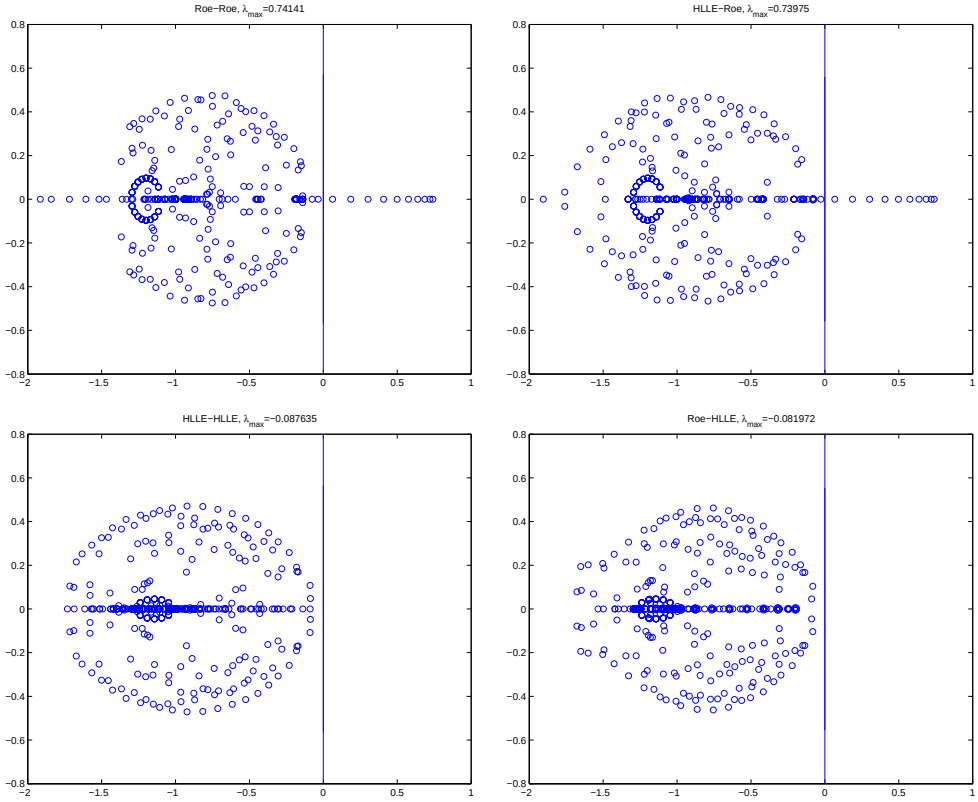


Figure 3: Eigenvalues of the stability matrix in the complex plane.

where $\beta_1>0$, $\beta_2>0$, $\beta_1+\beta_2=1$.

From intuition one regards that the hybrid schemes become more stable with the proportion of the $HLL$ flux being increased. The results of matrix stability analysis are consistent with such cognition, but behaviors are different. Fig. 4 gives the maximal real parts of the eigenvalues of some hybrid schemes as functions of $\beta_2$ and upstream Mach number $M_a$. These schemes include $Roe-RoeHLL$, $RoeHLL-RoeHLL$, $HLL-RoeHLL$. In the left figure Mach number is fixed $M_a$=7, and in the right one combination coefficient is fixed $\beta_2=0.6$. From the discussion above we can conclude that:

1. The maximal real parts of eigenvalue are almost the same for all the three flux solvers which have different $x$-direction flux functions but same $y$-direction fluxes. This fact shows once more that the flux solver in the $x$-direction is not an important factor to guarantee stability but important in the $y$-direction.

2. For a given shock strength, numerical schemes become stable gradually with increasing the component of $HLL$ in the $y$-direction flux functions.

3. The instabilities of hybrid schemes are in proportion to shock strength.

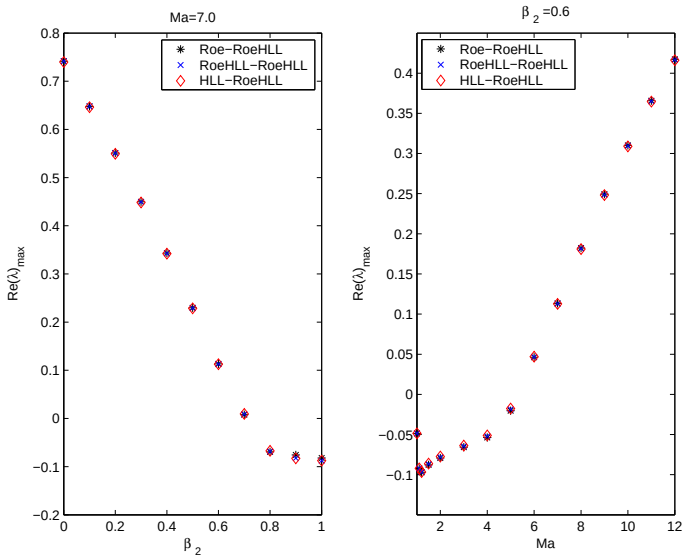


Figure 4: The maximal real part of the eigenvalues of the stability matrix vs. $\beta_2$ and Mach number.

## 5.2 Hybridization of flux components

Furthermore, we focus on which terms in the numerical fluxes are responsible for those numerical failings. For a scheme based on the Roe flux, if its $k^{th}$ component is replaced by a $HLL$ one, we denote it as $RoeHk$; if its $k_1^{th}$ and $k_2^{th}$ components are replaced by $HLL$ ones, we denote it as $RoeHk_1k_2$. The scheme $RoeHk_1k_2k_3$ may be defined by analogous manner. Two examples are

$$\begin{cases} H_{mk}^{RoeH3}(1)=H_{mk}^{Roe}(1); \\ H_{mk}^{RoeH3}(2)=H_{mk}^{Roe}(2); \\ H_{mk}^{RoeH3}(3)=H_{mk}^{HLL}(3); \\ H_{mk}^{RoeH3}(4)=H_{mk}^{Roe}(4), \end{cases} \qquad \begin{cases} H_{mk}^{RoeH13}(1)=H_{mk}^{HLL}(1); \\ H_{mk}^{RoeH13}(2)=H_{mk}^{Roe}(2); \\ H_{mk}^{RoeH13}(3)=H_{mk}^{HLL}(3); \\ H_{mk}^{RoeH13}(4)=H_{mk}^{Roe}(4). \end{cases}$$

The stabilities increase monotonically for successive $RoeHk_1$, $RoeHk_1k_2$ and $RoeHk_1k_2k_3$, which include common $HLL$ flux component $k_1$ and are consistent with intuitionistic knowledge. We omit stability analysis results here.

In what follows, we illustrate some interesting stability experiments. Firstly, we fix $x$-direction flux function as $Roe$ flux, and compare the stabilities of schemes $Roe-RoeHk$,$k$=1,2,3,4. Fig. 5 gives some maximal real parts of the eigenvalues of these schemes as function of upstream Mach number $M_a$. In these flux functions in $y$-direction, discrete form of tangent momentum equations plays an important role, and the $Roe-RoeH3$ is the only one scheme being stable for all Mach number. A further analysis shows that all the schemes $Roe-RoeHk_1k_2$ and $Roe-RoeHk_1k_2k_3$ are stable, provided that both of the sets $\{k_1,k_2\}$ and $\{k_1,k_2,k_3\}$ contain number 3, See Fig. 6.

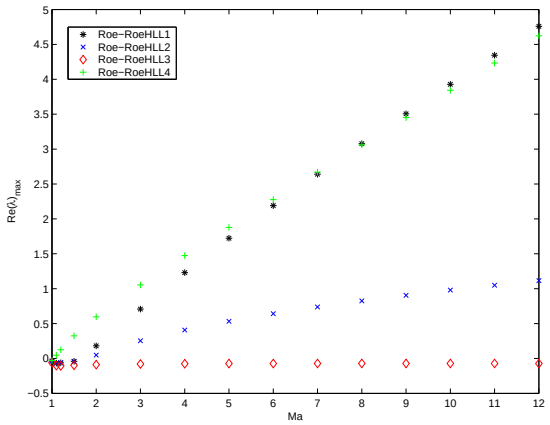


Figure 5: The maximal real part of the eigenvalues of the stability matrix vs. Mach number.

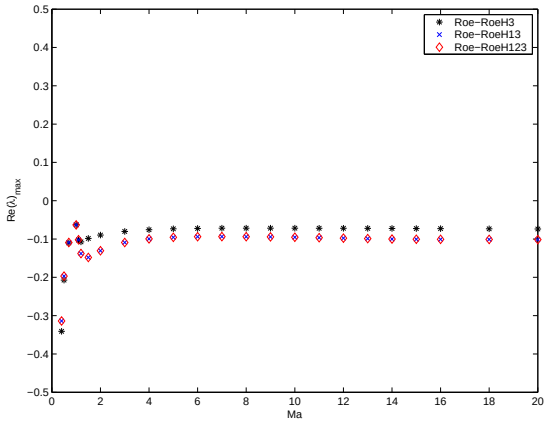


Figure 6: The maximal real part of the eigenvalues of the stability matrix vs. Mach number.

Finally, we hope to know what will happen in the case of lacking sufficient dissipation in the third component. Fix $x$-direction flux function as $HLL$ flux and observe the scheme $HLL-RoeH124$, which differs from the $HLL$ method only on discrete scheme of the third flux component at the edge normal to $y$-direction. The eigenvalue of the stability matrix for the scheme $HLL-RoeH124$ is 5.3201 at Mach number 7. This means that those schemes with $Roe$ flux function being as the third flux component are unstable.

In summary, a numerical scheme whose third flux component in $y$-direction is $HLL$ flux is always linear stable whatever the form of other fluxes are taken; and a numerical scheme is always linear unstable regardless of the form of other fluxes, provided that the third flux components in $y$-direction is the $Roe$ flux. Therefore the discrete form of this flux component ($\rho uv$) occupies a special position to the stability of scheme.

**Remark 5.1.** When neglecting the adaptation of coefficients, the stability analysis for the $Roe-RoeH13$ provides a theoretical foundation on the device of the fluxes (3.10).

### 5.3 Causes and consequences of instability

When fluids pass through shock without perturbations, according to Rankine-Hugoniot relations, the shear velocity $v$ and mass flux $\rho u$ keep to be continuous, whereas the other states $(\rho,u,p,E)$ come into being jumps. See Fig. 7(a) and (c).

Due to different disturbed situations, all conservation quantities $\rho,\rho u,\rho v,E$ may suffer errors during the jump procedure, and discrepancies of physical quantities in the transverse of shock might appear (see Fig. 7(b) and (d)). If these disturbed errors are controlled within a small range during the calculation, the scheme is stable, otherwise it is unstable. From the previous subsection we know that disturbances of quantities $\rho,\rho v,E$ in cells $(i,j)$ and $(i,j+1)$ do not cause instability even if the low dissipative *Roe* flux is adopted, but discrete form of the third flux component $\rho uv$ in $y$-direction is a sensitive and important factor to influence stability. Notice that the role of the flux component $\rho uv$ is to convect momentum $\rho u$ in the transverse of shock wave, we need to observe viscosity behavior of different schemes and discuss their effects to $\rho u$.

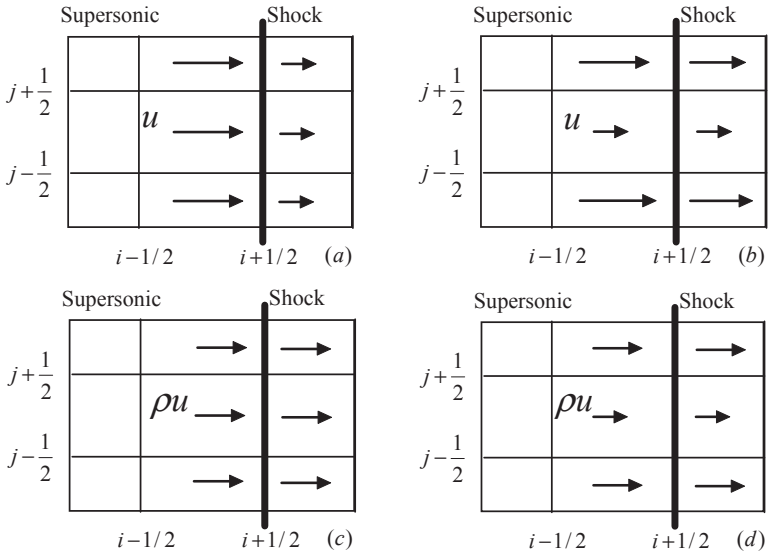


Figure 7: Normal velocity and momentum around shock without perturbations (a),(c) and with perturbations (b),(d). The root of numerical shock instability: the distribution of normal momentum $\rho u$ along shock front. (c) Stability; (d) instability.

Fig. 8 gives the wave structures of the *Roe* and $HLL$ schemes in $y$-direction. We use denotations in lab coordinate here, so transport velocity is $v$ and shear velocity is $-u$. The *Roe* solver has three characteristic waves with contact discontinuity and the $HLL$ solver only includes two nonlinear waves.

The update to momentum component $\rho u$ from $y$-direction is

$$(\rho u_y)_{i,j}^{n+1}=(\rho u)_{i,j}^{n}-\frac{\Delta t}{\Delta y}[(\rho uv)_{i,j+1/2}-(\rho uv)_{i,j-1/2}],$$

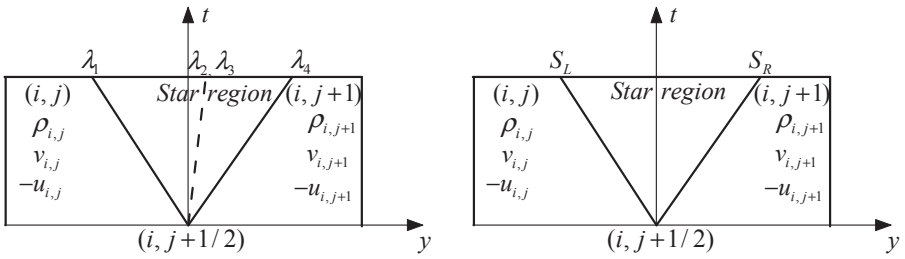


Figure 8: The wave structures of the *Roe* and *HLL* fluxes in the $y$-direction.

where $(\rho u_y)$ represents partial momentum obtained only from transport of $\rho u$ in $y$-direction. For brevity, we call $\rho u$ normal momentum because it is perpendicular to shock front.

The fluxes can be obtained by wave decomposition. Without loss of generalization, we assume eigenvalues $\lambda_1<0,\lambda_2=\lambda_3>0$ and $\lambda_4>0$ at edges $j\pm1/2$ and the signal speeds $S_L$ and $S_R$ of the $HLL$ solver coincide with $\lambda_1$ and $\lambda_4$ in the *Roe* solver. For the *Roe* scheme,

$$\begin{aligned}(\rho uv)_{i,j+1/2}&=(\rho uv)_{i,j}+(\lambda_1\hat{\alpha}_1\hat{u})_{i,j+1/2},\\(\rho uv)_{i,j-1/2}&=(\rho uv)_{i,j}-(\lambda_2\hat{\alpha}_2\hat{u}+\lambda_3\hat{\alpha}_3)_{i,j-1/2}-(\lambda_4\hat{\alpha}_4\hat{u})_{i,j-1/2},\end{aligned}$$

where the eigenvalues $\lambda_{1,2,3,4}=\{\hat{v}-\hat{c},\hat{v},\hat{v},\hat{v}+\hat{c}\}$, "$\hat{}$" means Roe-averaged value at the cell interface, and the wave strengthes are

$$\hat{\alpha}_{1,2,3,4}=\left\{\left(\frac{\Delta p-\hat{\rho}\hat{c}\Delta v}{2\hat{c}^2}\right),\left(\Delta\rho-\frac{\Delta p}{\hat{c}^2}\right),\hat{\rho}\Delta u,\left(\frac{\Delta p+\hat{\rho}\hat{c}\Delta v}{2\hat{c}^2}\right)\right\}.$$

Here $\Delta q_{i,j+1/2}=q_{i,j+1}-q_{i,j}$. Therefore the flux difference is

$$\begin{aligned}&-\left[(\rho uv)_{i,j+1/2}-(\rho uv)_{i,j-1/2}\right]\\&=-(\lambda_1\hat{\alpha}_1\hat{u})_{i,j+1/2}-(\lambda_2\hat{\alpha}_2\hat{u}+\lambda_3\hat{\alpha}_3)_{i,j-1/2}-(\lambda_4\hat{\alpha}_4\hat{u})_{i,j-1/2}\\&=-\left[(\hat{v}-\hat{c})\frac{\Delta p-\hat{\rho}\hat{c}\Delta v}{2\hat{c}^2}\hat{u}\right]_{i,j+\frac{1}{2}}-\left[\hat{v}(\Delta(\rho u)-\frac{\Delta p}{\hat{c}^2}\hat{u})\right]_{i,j-\frac{1}{2}}-\left[(\hat{v}+\hat{c})\frac{\Delta p+\hat{\rho}\hat{c}\Delta v}{2\hat{c}^2}\hat{u}\right]_{i,j-\frac{1}{2}}.\end{aligned}\quad(5.1)$$

For the $HLL$ scheme,

$$\begin{aligned}(\rho uv)_{i,j+1/2}&=(\rho uv)_{i,j}+\lambda_{1,i,j+1/2}[(\rho u)^*_{i,j+1/2}-(\rho u)_{i,j}],\\(\rho uv)_{i,j-1/2}&=(\rho uv)_{i,j}-\lambda_{4,i,j-1/2}[(\rho u)_{i,j}-(\rho u)^*_{i,j-1/2}],\end{aligned}$$

where the middle state $(\rho u)^*_{i,j+1/2}$ is

$$(\rho u)^*_{i,j+1/2}=\frac{\lambda_{4,i,j+1/2}(\rho u)_{i,j+1}-\lambda_{1,i,j+1/2}(\rho u)_{i,j}+(\rho uv)_{i,j}-(\rho uv)_{i,j+1}}{\lambda_{4,i,j+1/2}-\lambda_{1,i,j+1/2}}.$$

Then the flux difference is

$$\begin{aligned}&-\left[(\rho uv)_{i,j+1/2}-(\rho uv)_{i,j-1/2}\right]\\&=-\left[(\hat{v}-\hat{c})\frac{(\hat{v}+\hat{c})\Delta(\rho u)-\Delta(\rho uv)}{2\hat{c}}\right]_{i,j+\frac{1}{2}}-\left[(\hat{v}+\hat{c})\frac{\Delta(\rho uv)-(\hat{v}-\hat{c})\Delta(\rho u)}{2\hat{c}}\right]_{i,j-\frac{1}{2}}.\end{aligned}\tag{5.2}$$

The terms with subscript $j\pm1/2$ in (5.1) and (5.2) represent contribution from cells $j\pm1$, we only choose one side and discuss effect from cell $j-1$. Denote $\delta$ as amount of perturbation quantities, that means

$$\Delta p\sim\delta,\ \Delta u\sim\delta,\ \Delta v\sim\delta,\ \Delta(\rho u)\sim\delta,\ etc.$$

When advection velocity $\hat{v}=0$ or very small $\hat{v}\sim\delta$, the viscosity of linear contact wave in the *Roe* solver $-\hat{v}(\Delta(\rho u)-\Delta p\hat{u}/\hat{c}^2)\sim\delta^2$ is negligible. The contribution from nonlinear wave component

$$-(\hat{v}+\hat{c})\frac{\Delta p+\hat{\rho}\hat{c}\Delta v}{2\hat{c}^2}\hat{u}\sim-\frac{\Delta p+\hat{\rho}\hat{c}\Delta v}{2\hat{c}}\hat{u}$$

can not make sure to diminish the discrepancies of $\rho u$ between cells. In fact, $\Delta p$ and $\Delta v$ are independent of $\rho u$ and discrepancies of $\rho u$ may become larger than before. When advection velocity $v$ is large, the amount of dissipation of linear wave $-\hat{v}\Delta(\rho u)$ increases and helps to smear differences of $\rho u$. On the other hand, the $HLL$ scheme always includes viscosity to reduce the discrepancy $\Delta(\rho u)$ no matter the value of $v$. In fact, there is

$$-(\hat{v}+\hat{c})\frac{\Delta(\rho uv)-(\hat{v}-\hat{c})\Delta(\rho u)}{2\hat{c}}\sim-(\hat{v}+\hat{c})\frac{\hat{\rho}\hat{u}\Delta v+\hat{c}\Delta(\rho u)}{2\hat{c}},$$

here we use approximation $\Delta(\rho uv)\approx\hat{\rho}\hat{u}\Delta v+\hat{v}\Delta(\rho u)$. According to previous assumption that $\hat{v}=\lambda_2\geq0$, $-(\hat{v}+\hat{c})\Delta(\rho u)/2$ has opposite sign with $\Delta(\rho u)$.

Based on these analysis results, we can draw a conclusion: when fluids pass through a shock, the sawtooth form of normal momentum $\rho u$ along the transverse direction of the shock can cause instability of numerical shock, see Fig. 7(d). If a scheme has mechanism to average the discrepancies of $\rho u$, especially when transport velocity $v$ is close to zero, the linear stability will be improved (Fig. 7(c)).

Both density and normal velocity perturbations can result in large discrepancies of $\rho u$, therefore, both inconsistent distributions of density and normal velocity in the transverse direction of shock wave can be regarded as the sources of instability (Fig. 7(b)).

It is well known that the carbuncle instability exhibits sawtooth errors to all quantities (cf. [25]) in the transversal direction of shock wave. We attribute error distributions of other quantities to the consequences of shock instability and regard they are induced by instability coming from normal momentum perturbations.

When shock wave is not steady, the matrix stability analysis is invalid. For general cases (unsteady shock, irregular grid), one still may heuristically infer that instability is caused by the distribution of $\rho u$ in the transverse direction of shock wave. This claim is consistent with the numerical experiments in [22]. For example, both the increase of grid

number along a shock front and large velocity transition $\Delta u$ between a shock front can increase possibility to inconsistency of $\rho u$ in the transverse of the shock. They correspond to some other factors to influence stability such as large aspect ratio of a grid and shock strength. Imposing sufficient dissipation on transverse direction of shock wave is one applicable method to cure shock instability.

In the application of computational fluid dynamics, low dissipative schemes have special attraction due to their increased accuracy, in particular for boundary-layer or shear-layer computations. It is very difficult to reach a compromise between accuracy and robustness at the same time. Because the analysis proposed here is more detailed than before, it is possible to set appropriate viscosity in hybrid schemes to restrain carbuncle resource without degrading the accuracy too much, such as scheme (3.10). Such analysis is helpful for designing other better schemes which can remove some instability and keep accuracy as well.

# 6 Numerical behaviors of hybrid methods

## 6.1 Comparison of some hybrid methods

In Section 5, we have discussed the stabilities of some hybrid methods with fixed combination parameters $\beta_1$ and $\beta_2$. In this section, we will compare numerical behaviors for the solutions of some hybrid schemes when combination parameters vary. For the sake of brevity, we consider the hybrid methods with the following flux functions:

$$H_{mk}^{Modify}(\mathbf{n})=\begin{cases}\frac{\alpha_1}{\alpha_1+\alpha_2}H_{mk}^{Roe}(\mathbf{n})+\frac{\alpha_2}{\alpha_1+\alpha_2}H_{mk}^{HLL}(\mathbf{n}), & \text{if } |\Delta\mathbf{u}|>\varepsilon,\\ H_{mk}^{Roe}(\mathbf{n}), & \text{otherwise,}\end{cases} \tag{6.1}$$

$$H_{mk}^{Contra}(\mathbf{n})=\begin{cases}\frac{\alpha_1}{\alpha_1+\alpha_2}H_{mk}^{HLL}(\mathbf{n})+\frac{\alpha_2}{\alpha_1+\alpha_2}H_{mk}^{Roe}(\mathbf{n}), & \text{if } |\Delta\mathbf{u}|>\varepsilon,\\ H_{mk}^{Roe}(\mathbf{n}), & \text{otherwise,}\end{cases} \tag{6.2}$$

and rotated hybrid method (3.4), which is rearranged into following form

$$H_{mk}^{Rotate}(\mathbf{n})=\begin{cases}\alpha_1 T_1 H_{mk}^{HLL}(\mathbf{n}_1)+\alpha_2 T_2 H_{mk}^{Roe}(\mathbf{n}_2), & \text{if } |\Delta\mathbf{u}|>\varepsilon,\\ H_{mk}^{Roe}(\mathbf{n}), & \text{otherwise.}\end{cases} \tag{6.3}$$

Here $\mathbf{n}_{1,2}$ and $\alpha_{1,2}$ are defined in (3.1), $\varepsilon=10^{-12}$, $T_{1,2}$ are matrices

$$T_1=\begin{pmatrix}1&0&0&0\\0&\alpha_1&-\alpha_2&0\\0&\alpha_2&\alpha_1&0\\0&0&0&1\end{pmatrix},\quad T_2=\begin{pmatrix}1&0&0&0\\0&\alpha_2&\alpha_1&0\\0&-\alpha_1&\alpha_2&0\\0&0&0&1\end{pmatrix}.$$

Obviously the first flux function (6.1) is a modification of flux in the Wu et al.'s scheme (3.10). In the second flux function the combination coefficients are opposite with the first

one in flow region $|\Delta\mathbf{u}|>\varepsilon$. We call the three functions as 'modified flux', 'contrastive flux' and 'rotated flux' respectively.

Let's consider a grid-aligned shock wave with perturbations. It needs to point out that all the three hybrid methods keep robust and stable property for a wide of perturbation data. But stability mechanisms among these schemes are different because of the different hybrid manners.

Suppose that the velocity difference across a cell edge is decomposed into

$$\Delta\mathbf{u}=\Delta u_n\mathbf{n}+\Delta u_t\mathbf{t}=\alpha_1|\Delta\mathbf{u}|\mathbf{n}+\alpha_2|\Delta\mathbf{u}|\mathbf{t},$$

where $\mathbf{n},\mathbf{t}$ are unit normal and tangent vectors of the cell edge.

Firstly, let's see the distribution of $\alpha$ at different cell edge. For a cell edge aligns with shock wave (such as edge $i+1/2$ in Fig. 7), according to the Rankine-Hugoniot relations across a shock wave, the velocity difference normal to the cell edge ($\Delta u_n$) is usually greater than that parallel to the shock wave front ($\Delta u_t$), i.e., $\alpha_1>\alpha_2$. For a cell edge perpendicular to the shock surface (such as edge $j+1/2$), it is possible to have $\Delta u_n<\Delta u_t$ and $\Delta u_n>\Delta u_t$ due to perturbations. Therefore there are two cases at edge $j+1/2$: $\alpha_1<\alpha_2$ or $\alpha_1>\alpha_2$. Notice that shear velocity $u_t$ at the cell edge $j+1/2$ corresponds to $u$ in Fig. 7, and its inconsistent distribution $\Delta u_t$ along shock front is thought to be one of the sources of triggering instability.

Secondly let's compare the stability mechanisms of the three schemes. The modified hybrid flux (6.1) determines hybrid quotient of $HLL$ solver according to the proportion of $\alpha_2=\Delta u_t/|\Delta\mathbf{u}|$. It blends more *Roe* flux at shock surface, but is problem-dependent in the transverse direction of shock wave. When the perturbation $\Delta u_t$ at edge $j+1/2$ increases, the composition of the $HLL$ flux included in the hybrid scheme will increase automatically to introduce more viscosity. Therefore this method can reduce instability by restricting resource of instability directly.

The contrastive hybrid flux (6.2) increases quotient of the $HLL$ solver by $\alpha_1=\Delta u_n/|\Delta\mathbf{u}|$. It particularly suits to the calculation of shear flow which needs more *Roe* flux between front. But, it is possible to cause instability in shock problem, since it doesn't restrain transverse perturbation $\Delta u_t$ at edge $j+1/2$ directly. According to the analysis in the last subsection, the development of instability may lead to change of quotient of $\Delta u_n$. If proportion of $\Delta u_n$ increases, more $HLL$ viscosity at this edge is introduced and helps to damp discrepancies of normal momentum $\Delta(\rho u)$, then calculation is stable. If $\alpha_1$ keeps small all the time during perturbations development, shock instability will occur.

The rotated hybrid flux (6.3) has similar situations with (6.2). When $\alpha_1>\alpha_2$ such as at shock front, it includes more $HLL$ flux. At edge $j+1/2$ and $\alpha_1$ is very small, the consequence of instability evolving may amplify proportion of $\Delta u_n$ in $|\Delta\mathbf{u}|$ to suppress instability. Otherwise, insufficient dissipation may cause instability.

In summary, the stabilized approaches of the last two schemes (6.2) and (6.3) are indirect and undergo a procedure from instability to stability. The stability of schemes comes from the self-adaption of hybrid coefficients.

Different stability mechanisms lead to different solution behaviors for these numerical schemes. The last two schemes (6.2) and (6.3) have possibility to suffer instability in some special cases although they have passed through many stringent tests [20], while the scheme (6.1) keeps stability in all tests made by us.

In what follows, we give some numerical experiments with strong shock wave to illustrate our analysis results. It needs to point out that all results come from cell-centered finite volume method rather than node-centered scheme [20].

## 6.2 Mach 20 hypersonic flow over a cylinder

This is a well-known test to examine the catastrophic carbuncle failings of upwind schemes [22, 24, 29]. A Mach number 20 inviscid fluid flows around a circular cylinder, and both the initial density and pressure are 1. In this test problem, $40\times300$ and $40\times600$ structure grids and the first order accuracy schemes are used. The density contours at $t=3$ by three hybrid schemes are illustrated in Figs. 9 and 10. All of the three schemes are

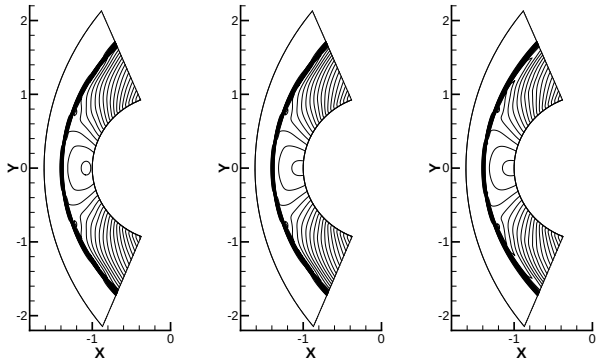


Figure 9: The contours of the density for hypersonic flow over a cylinder. Grid resolution is $40*300$. Left: the modified hybrid flux (6.1); middle: the contrastive hybrid flux (6.2); right: the rotated hybrid flux (6.3).

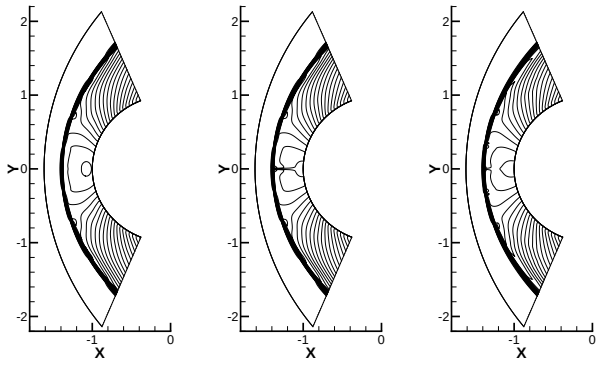


Figure 10: The contours of the density for hypersonic flow over a cylinder. Grid resolution is $40*600$. Left: the modified hybrid flux (6.1); middle: the contrastive hybrid flux (6.2); right: the rotated hybrid flux (6.3).

stable, but with the increasing of length-width ratio of mesh, the slight carbuncle phenomena appear when using contrastive hybrid flux (6.2) and rotated hybrid flux (6.3). The modified hybrid flux (6.1) still keeps stability very well.

### 6.3 Odd-even decoupling

Fig. 11 shows an odd-even decoupling test problem [25] using the hybrid schemes on quadrilateral mesh. A moving shock propagates to the right. Different from traditional shock with $Ma=6$, the initial value is set to be modified Noh's one [21], which has infinity shock strength:

$$\begin{aligned}\mathbf{W}_0 &= (\rho,u,v,p,\gamma)_0 = (1,0,0,0,5/3), \qquad x>20,\\ \mathbf{W}_1 &= (\rho,u,v,p,\gamma)_1 = (4,1,0,4/3,5/3), \quad x<20.\end{aligned}$$

The computational domain $800\times 20$ and the grid steplength is 1. The centerline of the grid is perturbed from a perfectly uniform grid by $\pm 10^{-3}$. We note the magnitude of perturbation is the same as that in [22] and larger than that used in [25] to emphasize the problem of shock instability. The initial position of the shock wave is at $x=20$ and shock velocity is $4/3$. The results show the density contour near $x\approx 290$ when $t=200$. The numerical shock obtained from the contrastive hybrid flux (6.2) is destroyed completely. The scheme (3.4) has better performance than (6.2) but shows the promotion of odd-even decoupling along the shock. The modified scheme (6.1) shows that the decoupling is completely eliminated.

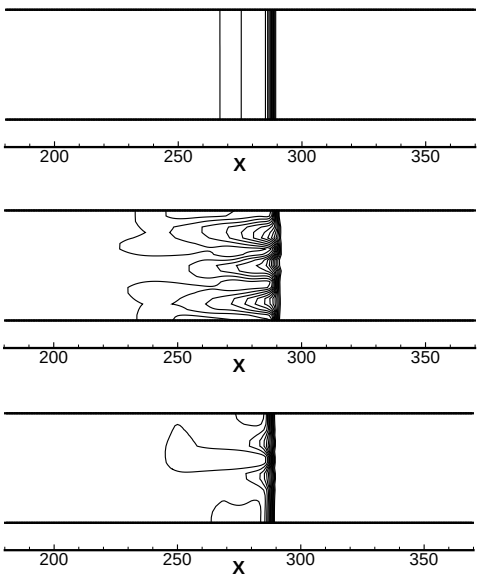


Figure 11: The contours of the density for the Noh problem. Upper: the modified hybrid flux (6.1); middle: the contrastive hybrid flux (6.2); bottom: the rotated hybrid flux (6.3).

### 6.4 Steady normal shock

We consider the same Noh problem [21] but with steady shock on the domain $[-0.5,0.5]\times[0,0.2]$. The initial values are

$$\begin{aligned}\mathbf{W}_0&=(\rho,u,v,p,\gamma)_0=(1,4/3,0,0,5/3), \qquad x<0,\\ \mathbf{W}_1&=(\rho,u,v,p,\gamma)_1=(4,1/3,0,4/3,5/3), \quad x>0.\end{aligned}$$

The resolution of the rectangular grid is $100\times20$. The initial values are given by random perturbations with order $10^{-6}$. The boundary conditions are the same as those in Subsection 4.1. Fig. 12 depicts the density contours given by the schemes (6.3) and (6.1). The rotated hybrid method (6.3) have solutions with shock propagating at nonzero speeds and modified method (6.1) keeps the steady shock very well.

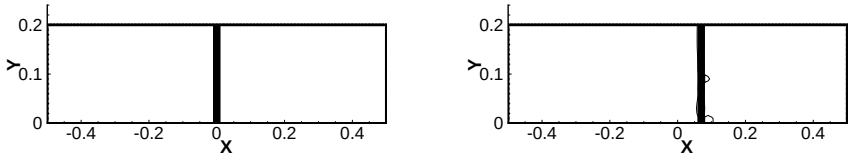


Figure 12: The contours of the density for a steady shock problem. Left: the modified hybrid flux (6.1); right: the rotated hybrid flux (6.3).

## 7 Summary

In this paper, a matrix-based stability analysis is performed to illustrate the stability of hybrid schemes. The background fluid is a steady shock. By combining the *Roe* with *HLL* flux along different directions, we show that the numerical shock instability comes from flux in transverse direction of shock wave. In this flux vector, only the discrete form of the flux component, which is responsible for convecting normal momentum along tangent direction of shock, can result in stability or instability. This fact makes us believe that the inconsistent normal momentum distribution along shock front is the source to cause instability. The sawtooth form of other physical quantities along shock front is the consequence of unstable computation.

Based on the results of stability analysis, we compare some hybrid schemes and illustrate their different stabilized mechanisms in controlling shock instability. Numerical experiments are presented to verify our analysis results. The conclusion is that the scheme of restricting directly instability source is indeed more stable than other hybrid schemes.

Although the analysis method succeeds in explaining strong shock problems, its limitation still exists due to the matrix analysis method itself. For example, it is not able to illustrate why the one dimensional shock structure may stabilize a numerical scheme even without transverse dissipation [2], and it does not explain why the Osher method with natural ordering of the eigenvalues become unstable with Mach numbers increasing

($>2.3$) but suddenly becomes stable for Mach numbers larger than 5.5 [4]. Furthermore researches need to be involved.

## Acknowledgments

This project is supported by the National Natural Science Foundation of China (11071025), the Foundation of CAEP (2010A0202010), the Foundation of National Key Laboratory of Science and Technology Computation Physics and the Defense Industrial Technology Development Program (B1520110011). The authors thank the reviewers' valuable suggestions during the revision of paper.

### References

[1] P. Chandrashekar, Kinetic energy preserving and entropy stable finite volume schemes for compressible Euler and Navier-Stokes equations, Commun. Comput. Phys., 14 (2013), 1252-1286.
[2] Y. Chauvat, J. M. Moschetta and J. Gressier, Shock wave numerical structure and the carbuncle phenomenon, Int. J. Numer. Meth. Fluids 47, 2005, 903-909.
[3] S.F. Davis, A rotationally biased upwind difference scheme for the Euler equations, J. Comput. Phys., 56 (1984), 65-92.
[4] M. Dumbser, J. M. Morschetta, J. Gressier, A matrix stability analysis of the carbuncle phenomenon, J. Comput. Phys., 197 (2004), 647-670.
[5] M. Dumbser and E. F. Toro, On universal Osher-type schemes for general nonlinear hyperbolic conservation laws, Commun. Comput. Phys., 10(2011), 635-671.
[6] S. K. Godunov, A finite difference method for computation of discontinuous solutions of the equations of fluid dynamics. Mat. Sb., 47 (1959), 271-306.
[7] J. Gressier and J. M. Moschetta, Robustness versus accuracy in shock-wave computations, Int. J. Numer. Meth. Fluid., 33 (2000), 313-332.
[8] A. Harten and J. M. Hyman, Self adjusting grid methods for one dimensional hyperbolic conservation laws, J. Comput. Phys., 50 (1983), 235-269.
[9] A. Harten, P. D. Lax and B. van Leer, On upstream differencing and Godunov-type schemes for hyperbolic conservation laws, SIAM Review, 25 (1983), 35-61.
[10] P. Janhunen, A positive conservative method for magnetohydrodynamics based on HLL and Roe methods, J. Comput. Phys., 166 (2000), 649-661.
[11] F. Kemm, A note on the carbuncle phenomenon in shallow water simulations, ZAMM – Journal of Applied Mathematics and Mechanics, DOI: 10.1002/zamm.201200176
[12] S. S. Kim, C. Kim, O. H. Rho and S. K. Hong, Cures for the shock instability: development of a shock-stable Roe scheme, J. Comput. Phys., 185 (2003), 342-374.
[13] S. D. Kim, B. J. Lee, H. J. Lee, I. Jeung, Robust HLLC Riemann solver with weighted average flux scheme for strong shock,J. Comput. Phys., 228 (2009), 7634-7642.
[14] K. Kitamura, P. Roe and F. Ismail, Evaluation of Euler Fluxes for Hypersonic Flow Computations, AIAA JOURNAL, 47(1) (2009), 44-53.
[15] D. W. Levy, K. G. Powell, B. van Leer, Use of a rotated Riemann solver for the two-dimensional Euler equations, J. Comput. Phys., 106 (1993), 201-214.

[16] J. Q Li, Q. B. Li, K. Xu, Comparison of the generalized Riemann solver and the gas-kinetic scheme for inviscid compressible flow simulations, J. Comput. Phys., 230 (2011), 5080-5099.
[17] M. S. Liou and C. J. Steffen, A new flux splitting scheme, J. Comput. Phys., 107 (1993), 23-39.
[18] M. S. Liou, Mass Flux schemes and connection to shock instability, J. Comput. Phys., 160 (2000), 623-648.
[19] J. M. Moschetta, J. Gressier, J. C. Robinet, G. Casalis, The Carbuncle Phenomenon: a Genuine Euler Instability?, in Godunov Methods, Theory and Applications, Ed. E.F. Toro, Kluwer Academic/Plenum Publ., (1995), 639-645.
[20] H. Nishikawa and K. Kitamura, Very simple, carbuncle-Free, Boundary-Layer-Resolving, Rotated-Hybrid Riemann Solvers, J. Comput. Phys., 227 (2008), 2560-2581.
[21] W. F. Noh, Errors for calculations of strong shocks using an artificial viscosity and an artificial heat flux, J. Comput. Phys., 72 (1987) 78-120.
[22] M. Pandolfi and D. D'Ambrosio, Numerical instabilities in upwind methods: analysis and cures for the carbuncle phenomenon, J. Comput. Phys., 166 (2001), 271-301.
[23] S. H. Park, J. H. Kwon, On the dissipation mechanism of Godunov-type schemes, J. Comput. Phys., 188 (2003), 524-542.
[24] K. M. Peery and S. T. Imlay, Blunt-Body Flow Simulations, AIAA Paper 88-2904, 1988.
[25] J. Quirk, A contribution to the Great Riemann Solver Debate, Int. J. Numer. Meth. Fluid., 18 (1994), 555-574.
[26] Y. X. Ren, A robust shock-capturing scheme based on rotated Riemann solvers, Computers & Fluids, 32 (2003), 1379-1403.
[27] J. Robinet, J. Gressier, G. Casalis and J.-M. Moschetta, Shock wave instability and carbuncle phenomenon: same intrinsic origin?, J. Fluid Mech., 417 (2000), 237-263.
[28] P. L. Roe, Approximate Riemann solvers, parameter vector and difference schemes, J. Comput. Phys., 43 (1981), 357-372.
[29] R. Sanders, E. Morano and M. Druguet, Multidimensional dissipation for upwind schemes: stability and applications to gas dynamics, J. Comput. Phys., 145 (1998), 511-537.
[30] A. L. Scandaliato and M. S. Liou. AUSM-based high-order solution for Euler equations. Commun. Comput. Phys., 12 (2012), 1096-1120.
[31] E. F. Toro, M. Spruce and W. Speares, Restoration of the contact surface in the HLL-Riemann solver, Shock Wave, 4 (1994), 25-34.
[32] Y. Wada and M. S. Liou, An accurate and robust flux splitting scheme for shock and contact discontinuities, SIAM J. Sci. Comput., 18(3) (1997), 633-657.
[33] Y. Wada and M. S. Liou, A Flux Splitting Scheme with High-Resolution and Robustness for Discontinuities, NASA T. M. 106452 (1994).
[34] H. Wu, L. J. Shen, Z. J. Shen, A hybrid numerical method to cure numerical shock instability, Commun. Comput. Phys., 8(5) (2010), 1264-1271.
[35] K. Xu, Z. Li, Dissipative mechanism in Godunov-type schemes, Int. J. Numer. Methods Fluids, 37 (2001), 1-22.